Modeling and simulation for leg-wheel mobile robots using Modelica

Hiroki Yoshikawa Takatsugu Oda Kenichiro Nonaka Kazuma Sekiguchi

Tokyo City University, Japan, {g1681237,g1591201,knonaka,ksekiguc}@tcu.ac.jp

Abstract

Modeling of complex robots which consist of mechanical and electric elements has attracted a lot of attention to be utilized for analysis, simulation and development. In this paper, we model the space exploration robot which has leg-wheel mechanisms using Modelica, which is an equation based language and convenient to cope with a complex physical system. In addition, to evaluate the performance of planetary exploration robots, we conduct simulations considering the space environment using the fundamental control system and the robot model. The simulation results indicate that considering load shift due to centrifugal force is important under low gravitational acceleration. *Keywords: leg-wheel mobile robots, modeling,space robots, control system*

1 Introduction

Leg-wheel mobile robots dipicted in Figure 1 attract a lot of attention and are widely developed, because the robots achieve high stability utilizing leg mechanism and high mobility using wheel mechanism. Leg-wheel hybrid platform Quattroped, which has two degree-of-freedom legs, is developed (Shen et al., 2009). In order to climb up onto the steps, the control method for limb mechanism robot ASTERISK is studied (Fujii et al., 2006). The action planning algorithm for a planetary explorer robot LEON is proposed (Rohmer et al., 2010). Since these robots can move on uneven terrain, it is expected to work in planetary exploration. However, conducting experiments in space environment require too much cost and time. Therefore, simulating the robot behavior in space environment appears as a practical choice.

Figure 1. Leg-wheel mobile robots.

Equation based language Modelica is very efficacious to model complex systems which have mechanical and electrical elements. Several studies have reported the modeling and simulation results of several industrial applications using Modelica (Otter et al., 2015)(Hirano et al., 2015). In this paper, we model and simulate the behavior of a leg-wheel mobile robot modeled using geometric parameters of ATHLETE which has the leg-wheel mechanism developed by NASA (Wilcox et al., 2007) in the space environment using Modelica.

2 Modeling leg-wheel mobile robot

2.1 Outline

Table 1 shows the characteristics of the leg and the wheel mechanism. The moving speed and efficiency of the wheel mechanisms is higher than that of the leg mechanisms. The robots equipped with the leg mechanisms can move on uneven terrain. Moreover, the leg robots which have the redundancy in leg arrangement can control the wheel position to avoid overturn. The leg-wheel mobile robots possess both characteristics which enhance the robot mobility. In this paper, we focus on the ATHLETE as a typical example of leg-wheel mobile robot.

The ATHLETE is a lunar exploration robot developed by NASA. The leg-wheel mechanisms with six degree-of-freedom consisting of the wheel mechanism and the six joints are mounted on each vertex of the hexagonal body. The ATHLETE is able to allocate loads and move on uneven terrain while maintaining the body horizontally. These leg-wheel mechanisms are utilized in order to accommodate a wide range of tasks.

Table 1. Characteristics of leg-wheel mobile robots

	Leg	Wheel	leg-wheel
Climbing steps	Good	NG	Good
Load sharing	Good	NG	Good
Moving speed	OK	Good	Good

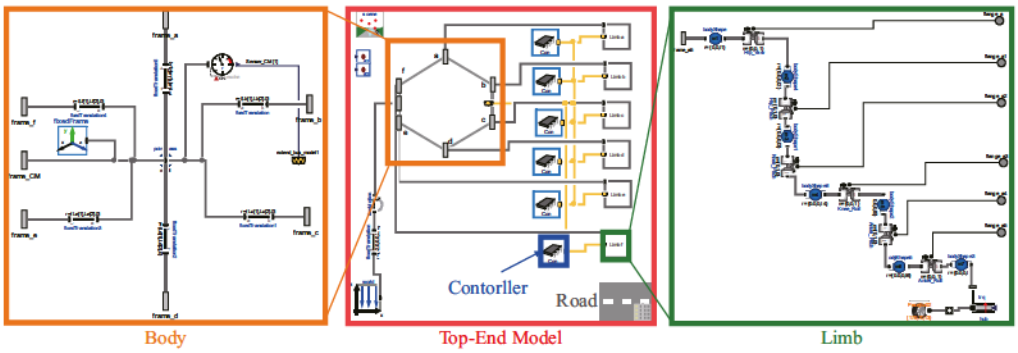

Figure 2. Top-end of Modelica model in Dymola.

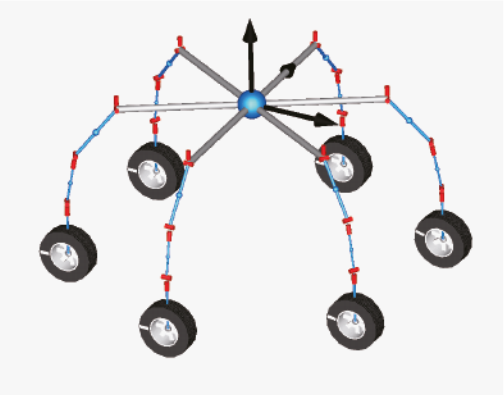

Figure 3. Leg-wheel mobile robot model.

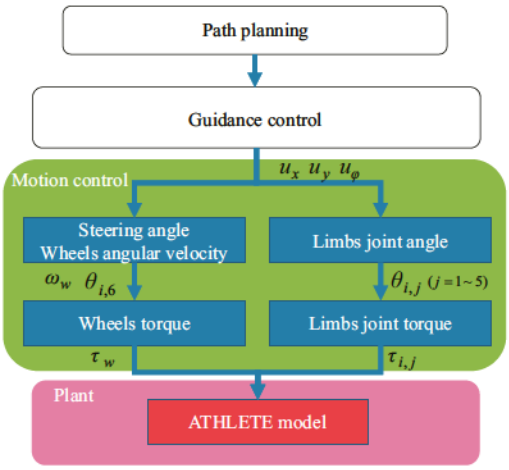

Figure 4. Control system flow.

2.2 Modeling

We model the leg-wheel robot which consists of body and limb-parts using Modelica in order to simulate the behavior of the wheel mechanism and analyze the mobility of ATHLETE. The ATHLETE model described by Modelica is shown in Figure 2 and 3. The robot model is designed as a rigid hexagonal body (orange frame) and links (green frame), as Figure 2 indicates. The body mass point which is the gravity center of the hexagon is set as the origin of the robot coordinate system (black arrows in Figure 3). A leg-wheel mechanism part consists of six revolute joints, seven links and the wheel mechanism. The limb mass points are set on the center of the wheel and the middle of each link. The tire model of Vehicle Dynamics Library (VDL) of Dymola is introduced to reproduce the actual wheel behavior.

3 Structure of the controller

3.1 Outline

As Figure 4 indicates, the controller consists of three layers: path planning layer, guidance control layer, and motion control layer. In this paper, the fundamental control system is proposed to achieve the reference vehicle velocity in the motion control layer. The motion control layer consists of two parts. First one is the control system for driving and steering of each wheel. Another part determines the posture of the robot. Details of each block are explained in the following sections.

3.2 Motion controller

In this section, we explain the leg-wheel mobile robot model and a calculation method of the controller. Figure 5 depicts the model of the leg-wheel robot. X_0 Y_0 is the inertial coordinate system and x y is the coordinate system fixed to the robot. (X_g, Y_g) is the position of the robot center of gravity (CoG) on the X_0 Y_0 coordinate system and ϕ is the orientation of the robot. u_x, u_y are the command translational velocity at CoG and u_ϕ is the command angular velocity on the x y coordinate system.

Figure 6 shows the configuration of the leg-wheel mechanism of the ATHLETE and the definition of the angle and torque of the leg joints. $\theta_{i,j}$ are the rotation angle of each joint where subscript $i = 1$ 6 indicates the legs number and $j = 1$ 6 indicates joint names of Hip Yaw, Hip Pitch, Knee Pitch, Knee Roll, Ankle Pitch, and Ankle Roll, respectively. In this paper, the Ankle Roll angle $\theta_{i,6}$ is controlled considering moving direction and

DOI 10.3384/ecp1612455

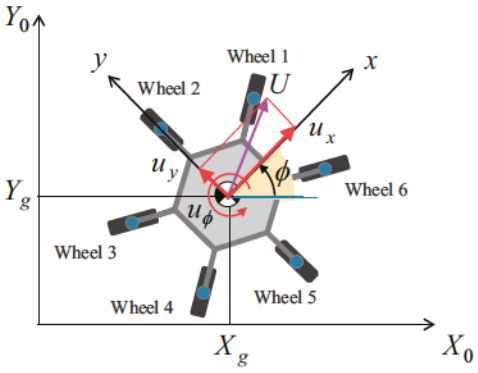

Figure 5. Top-view of plant model.

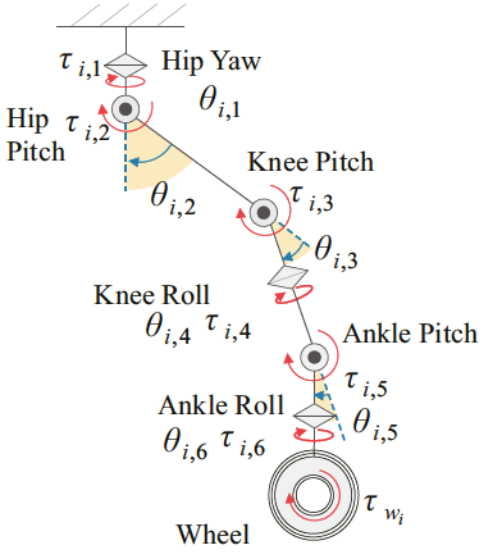

Figure 6. Configuration of limb joints of ATHLETE.

the other angles $\theta_{i,1}$ •••$\theta_{i,5}$ are controlled to maintain the reference posture.

Figure 7 shows the wheel and the Ankle Roll angle corresponding to the steering angle. $\theta_{i,0}$ is the angle from the CoG position to the wheel.

The translational velocities of the wheel $v_{x,i}$ and $v_{y,i}$ are calculated based on the command velocity at CoG u_x, u_y and u_ϕ as follows:

$$v_{x,i} = u_x \quad y_i u_\phi, \tag{1}$$
$$v_{y,i} = u_y + x_i u_\phi. \tag{2}$$

Reference angle $\hat{\theta}_{i,6}$ and angular velocity of wheel $\hat{\omega}_{wi}$ are calculated as follows:

$$\hat{\theta}_{i,6} = \tan^{1}\left(\frac{v_{y,i}}{v_{x,i}}\right) \quad \theta_{i,0}, \tag{3}$$
$$\hat{\omega}_{wi} = V_i / R_w, \tag{4}$$
$$V_i = v_{x,i}\cos\hat{\theta}_{i,6} + v_{y,i}\sin\hat{\theta}_{i,6}, \tag{5}$$

where R_w is a radius of the wheel and V_i is translational angular velocity. In order to achieve the reference angle

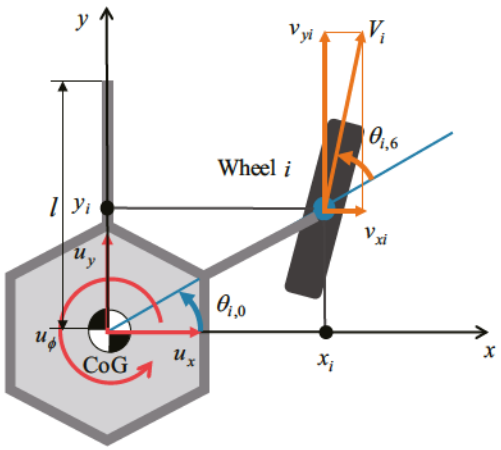

Figure 7. Velocity vector of wheel.

$\hat{\theta}_{i,j}$ and angular velocity $\hat{\omega}_{wi}$, we introduce the PD and P control as follows:

$$\tau_{i,j} = P_{th}(\hat{\theta}_{i,j} \quad \theta_{i,j}) + K_d(\hat{\dot{\theta}}_{i,j} \quad \dot{\theta}_{i,j}), \tag{6}$$
$$\tau_{wi} = P_w(\hat{\omega}_{wi} \quad \omega_{wi}), \tag{7}$$

where P_{th} and P_w are a proportional gain and K_d is a derivative gain.

Zero moment point (ZMP) is a one of concept which is an index of stability. When the ZMP position of the robot is kept inside the support polygon, the stability of the robot body is assured. We introduce the turning limit radius $r_{\max}$ considering rolling moment and ZMP position in order to evaluate the relationship between the height of CoG and centrifugal force. If the ZMP position coincides with the tip of the wheel position, the situation of the robot is regarded as a limitation of overturn. In this situation, the turning limit radius $r_{\max}$ is calculated as follows:

$$r_{\max} = \frac{{u_x}^2 z_c}{g\,l}, \tag{8}$$

where z_c is the height of the robot CoG, $l = \sqrt{{x_i}^2 + {y_i}^2}$ is the length from CoG position to the wheel position and g is gravitational acceleration.

4 Simulation

4.1 Conditions

To analyze robot behavior in the space environment, we conduct three simulations with the following conditions:

- Case 1 : Turning under the lunar gravity with the height of CoG high (Z_{CoG}=1.45 m)
- Case 2 : Turning under the lunar gravity with the height of CoG low (Z_{CoG}=0.866 m)

∼ Case 3 : Turning under the earth gravity with the height of CoG high (Z_{CoG}=1.45 m)

Comparing case 1 with 2, we analyze the effect of height of CoG z_{CoG}. The ATHLETE is able to change the height of CoG z_{CoG} by taking advantage of the redundancy of the leg joints. In these simulations, the height of CoG is changed so that the posture of the ATHLETE is maintained. Comparing case 1 with 3, we analyze the influence of the gravitational acceleration while turning. Physical parameters of the ATHLETE are determined based on the reference thesis (Wilcox et al., 2007). Commanded velocities are $\hat{u}_x = 2.5$ m/s, $\hat{u}_y = 0.0$ m/s, and $\hat{u}_\phi = \sqrt{\hat{u}_x^2 + \hat{u}_y^2}/R$. The turning radius R is designed to change smoothly using third-order polynomial from $R = 1000$ m to $R = 2.5$ m in 30 s. These commanded velocities generate a spiral trajectory that the turning radius is gradually decreased.

4.2 Results and Discussion

Figure 8, 9, and 10 show simulation results of case 1, 2 and 3, respectively. Figure 8 (a) and 9 (a) depict the trajectory of the robot, (b) depict the translational and rotational velocity, (c) depict body sideslip angle and (d) depict a vertical load of each wheel F_z. Figure 10 (a) depicts translational and rotational velocity and (b) depicts a vertical load of each wheel F_z.

As shown in Figure 8 (a), when the height of CoG is high, the robot can turn without overturn, however, the robot velocity has the error between commanded and actual velocity, as Figure 8 indicates. It is reasonable that the sideslip angle is generated, as Figure 8 (c) indicates. Since the velocity u_y is caused by centrifugal forces, the body sideslip angle arises. Figure 8 (d) indicates that the vertical load is distributed to each wheel ununiformly. Among them, limb 5 supports 70 % of the total load. The vertical load of limb 1 and 4 are equal to zero. It indicates that the robot is running using only four limbs. As shown in Figure 9 (a), when the height of CoG is lower than in case 1, the robot also can turn successfully. Figure 9 (b)(c) indicate that the tendency of velocity and body sideslip angle are similar to case 1. It is noteworthy that the load shift due to centrifugal force is suppressed, as Figure 9 (d) indicates. The reason is reducing the effect of rolling moment caused by the centrifugal forces. As shown in Figure 10 (a)(b), when gravitational acceleration is smaller than in case 1 and 2, the velocities are realized by the command velocity ; the robot does not generate the sideslip angle. In case 3, the influence of rolling moment generated by the centrifugal forces is smaller than case 1 and 2. It is because the gravitational acceleration works to suppress the roll rotational movement.

To evaluate these simulation results, we discuss the limit turning radius $r_{\max}$. At the turning radius of $r_{max} = 3.03$ m, the robot will fall down due to centrifugal force in the case 1. The robot is not overturn but some wheels are floating at the target turning radius of $R = 2.5$ m which is smaller than the limit turning radius r_{max} in case 1. On the other hand, when the target turning radius is modified to $R = 3.1$ m in case 1, all wheels contact with the load surface. There is little error between the limit and target turning radius within 0.1 m in this case, even though Eq. (8) assumes simplified model. Thus, we obtain the adequate simulation results. We can use the relationship of balance of moment for the control. It is expected that the turning ability in case 2 and 3 is better than that of case 1 by Eq. (8), because the limit turning radius decreases as gravitational acceleration increases and the height of CoG decreases. Accordingly, the simulation results indicate that the ZMP position close to the CoG position (X_g, Y_g) by suppressing the load shift of the robot.

The robot tends to generate skid in lunar space where the effects of gravitational acceleration are smaller than that of the earth. These results indicate that in order to achieve high mobility under the lunar environment, considering the sideslip angle and load shift is important, because the robot tends to overturn under low gravitational acceleration. To suppress load shift by centrifugal forces, leg-wheel mobile robots can lower the height of CoG using the leg mechanism. In addition, arranging the wheel position, the leg-wheel mobile robots can achieve high mobility utilizing the redundancy of the leg mechanism.

5 Conclusions

In this paper, we model the leg-wheel mobile robots which have the leg-wheel mechanism using Modelica and conduct the simulation considering the lunar environment. The simulation results indicate that the robots tend to generate the vehicle sideslip which is the cause for load shift and overturn because of low gravity acceleration. Therefore, the motion controller, which considers vehicle slippage, is required to achieve high mobility.

The future directions of this study are designing guidance controller, modeling motor dynamics, and considering a terramechanics which express the effects between wheel and sand called regolith.

6 Acknowledgments

The authors gratefully acknowledge the support of Grant in Aid for Scientific Research (C) No.15K06155 of Japan.

References

Shota Fujii, Tomohito Takubo, and Tatsuo Arai. Climbing up onto steps for limb mechanism robot "ASTERISK". In *International Association for Automation and Robotics in Construction*, pages 225–230, 2006.

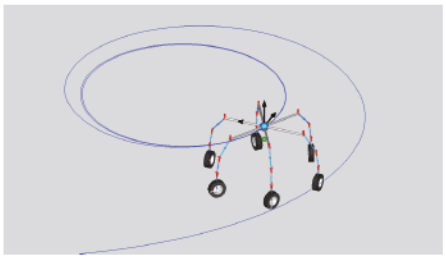

(a) Torajectory (until 40 s).

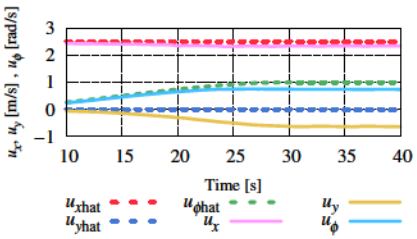

(b) Transrational and rotational velocity.

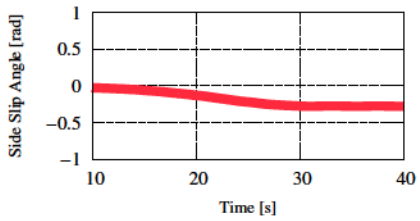

(c) Body sideslip angle.

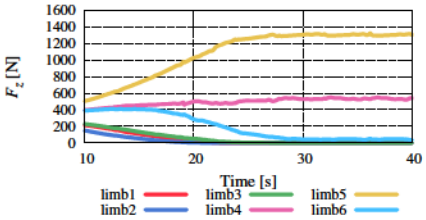

(d) Vertical load of each wheel.

Figure 8. Case 1 -High Center of gravity with the lunar gravitational acceleration- (R=2.5, z_{CoG}=1.45, g=1.65)

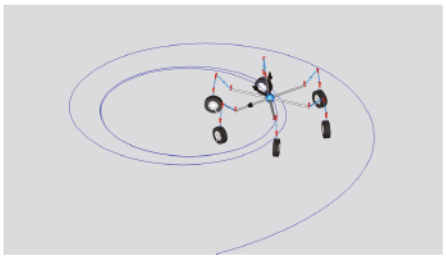

(a) Torajectory (until 40 s).

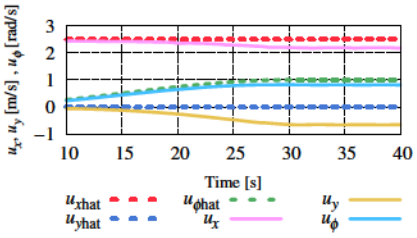

(b) Transrational and rotational velocity.

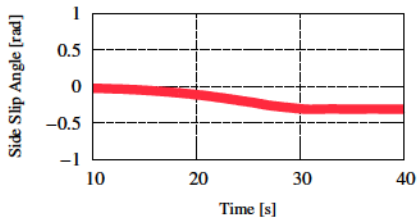

(c) Body sideslip angle.

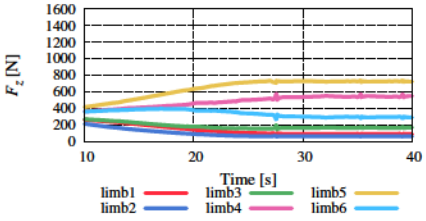

(d) Vertical load of each wheel.

Figure 9. Case 2 -Low Center of gravity with the lunar gravitational acceleration- (R=2.5, z_{CoG}=0.886, g=1.65)

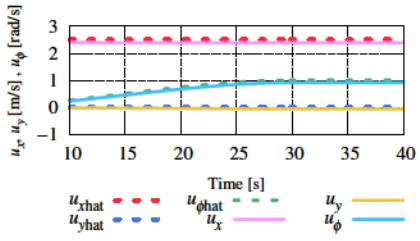

(a) Transrational and rotational velocity.

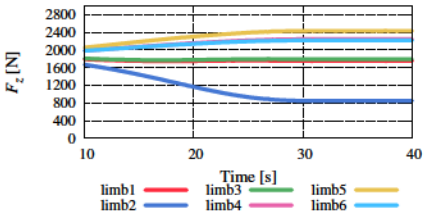

(b) Vertical load of each wheel.

Figure 10. Case 3 -High Center of gravity with the earth gravitational acceleration- (R=2.5, Z_{CoG}=1.45, g=9.81)

Yutaka Hirano, Shintaro Inoue, and Junya Ota. Model based development of future small electric vehicle by modelica. In *11th International Modelica Conference*, pages 143–150, 2015.

Martin Otter, Nguyen Thuy, Daniel Bouskela, Lena Buffoni, Hilding Elmqvist, Peter Fritzson, Alfredo Garro, Audrey Jardin, Hans Olsson, Maxime Payelleville, Wladimir Schamai, Eric Thomas, and Andrea Tundis. Formal requirements modeling for simulation-based verification. In *11th International Modelica Conference*, pages 625–635, 2015.

Eric Rohmer, Giulio Reina, and Kazuya Yoshida. Dynamic simulation-based action planner for a reconfigurable hybrid leg-wheel planetary exploration rover. *Advanced Robotics*, 24, 2010.

Shuan-Yu Shen, Cheng-Hsin Li, Chih-Chung cheng, Jau-Ching Lu, Shao-Fan Wang, and Pei-Chun Lin. Design of a leg-wheel hybrid mobile platform. In *IEEE/RSJ International Conference on Intelligent Robots and Systems*, pages 4682–4687, 2009.

Brian H. Wilcox, Todd Litwin, Jeff Biesiadecki, Jaret Matthews, Matt Heverly, Jack Morrison, Julie Townsend, Norman Ahmad, Allen Sirota, and Brian Cooper. ATHLETE: A cargo handling and manipulation robot for the moon. *Journal of Field Robotics*, 27(5):421–434, 2007.

DOI 10.3384/ecp1612455